Contents lists available at ScienceDirect

Applied Catalysis B: Environmental

Selective hydrogenation of CO2 into CO on a highly dispersed nickel catalyst obtained by magnetron sputtering deposition: A step towards liquid fuels

Renato V. Gonçalves [a,*], Lucas L.R. Vono [b], Robert Wojcieszak [c], Carlos S.B. Dias [d], Heberton Wender [e], Erico Teixeira-Neto [f], Liane M. Rossi [b,*]

[a] São Carlos Institute of Physics, University of São Paulo, PO Box 369, 13560-970, São Carlos, SP, Brazil
[b] Departamento de Química Fundamental, Instituto de Química, Universidade de São Paulo, Av. Professor Lineu Prestes 748, São Paulo, 05508-000, SP, Brazil
[c] Univ. Lille, CNRS, Centrale Lille, ENSCL, Univ. Artois, UMR 8181 – UCCS – Unité de Catalyse et Chimie du Solide, F-59000, Lille, France
[d] Brazilian Synchrotron Light Laboratory (LNLS), Campinas, SP, Brazil
[e] LNNano, Campinas, Brazil
[f] Electron Microscopy Laboratory, LNNano-CNPEM, P.O. Box 6192, 13083-970, Campinas, SP, Brazil

ARTICLE INFO

ABSTRACT

The transformation of CO_2 into CO through the reverse water gas shift (RWGS) reaction is very sensitive to the metal particle size and metal-support interactions. Indeed, large metallic particles or aggregates tend to produce more methane than CO. In this context, magnetron sputtering deposition was explored here for the preparation of highly dispersed nickel catalyst supported on silica. The Ni catalyst prepared for 30 min of sputtering time contains 2.4 wt% of Ni, small metal particles size (2.3 nm) and controlled composition (77% Ni, 23% Ni oxides). In-situ XANES under RWGS reaction conditions indicates reduction of nickel in the temperature range from 250 to 500 °C. The conversion of CO_2 into CO through the RWGS reaction was close to the thermodynamic equilibrium values for 1:1 and 1:4 (CO_2:H_2) gas composition at temperature as high as 800 °C. CO was produced continuously for 40 h at 660 °C without significant drop of activity. The overall catalytic performance was superior to that of a classical catalyst prepared by incipient wetness impregnation, as evidenced by the higher activity at T > 600 °C and stability for a long time on stream.

© 2017 Elsevier B.V. All rights reserved.

1. Introduction

Technologies for carbon capture and usage are being developed to mitigate the negative impacts of overly produced CO_2 and at the same time to produce renewable chemicals and fuels [1,2]. There are several chemical processes in which CO_2 can be used in the chemical industry [3,4]. However, the maximum amount of CO_2 that could be consumed for its conversion into chemicals represents only a small portion of the total CO_2 emissions. On the other hand, the utilization of CO_2 to produce hydrocarbon fuels could contribute significantly to the CO_2 mitigation [5,6].

The conversion of CO_2 into fuels could be done using different approaches, which mainly involve the production of CO and its subsequent conversion into hydrocarbons via Fischer–Tropsch (FT) synthesis. Reverse water gas shift (RWGS) is one of the most established reactions to convert CO_2 into CO and water [7–9]. However, it is an equilibrium-limited endothermic reaction that is favored at high temperatures [10,11]. In some cases, the products must be removed to shift the equilibrium toward the RWGS rather than the forward WGS [7]. In addition, methane is commonly formed as an undesired side product. At low temperatures (<600 °C) methane is the thermodynamic product. Catalysts usually used for this reaction are based on supported noble metals (e.g., Pt, Ru, and Rh) [12,13] and non-noble metals (e.g. Cu and Ni) [10,14–23]. Despite their low stability and usually poor selectivity, the non-noble metals catalysts are preferred for this reaction from the economic point of view. The catalyst performances in the RWGS reaction are governed by the physical and chemical properties of the active metal phase, and generally are very sensitive to the metal particle size which determines its dispersion on the support [19,24–26]. It has been shown that large metallic particles or aggregates, obtained at high metal loadings, decreased the RWGS selectivity and tended to produce more CH_4 (methanation reaction) [20,27,28].

In this context, the development of a general catalyst preparation method, which would be applicable for the preparation of highly dispersed noble and non-noble metals over several supports remains of great interest in view of optimizing the efficiency and cost-effectiveness of catalytic processes. Here, we describe a versatile method to prepare silica supported nickel nanoparticles (NPs) via a magnetron sputtering deposition method, which involves ejecting atoms and/or atomic clusters from highly pure targets (99.99%) onto a solid substrate [29–34]. The metal loading can be fine-tuned by controlling the sputtering time, while the particles size distribution is less affected if compared to the typical wet-impregnation methods [35]. The method can be applicable to different supports and metal targets, and also allows the combination of more than one metal. It is particularly attractive for the preparation of non-noble metals, providing M(0) nanoparticles, without using stabilizing agents that will contaminate the nanoparticle surface. The Ni-catalyst developed here by the magnetron sputtering method exhibits small metal particles size with controlled composition, which resulted in high selectivity for the RWGS reaction, conversion close to the thermodynamic equilibrium at high temperature and stability for a long time on stream.

2. Experimental

2.1. Chemicals

Tetraethyl orthosilicate (TEOS), polyoxyethylene(5) isooctylphenyl ether (IGEPAL CO-520), and ammonium hydroxide (NH$_4$OH) were purchased from Sigma-Aldrich (USA); ethanol and cyclohexane were purchased from Synth (Brazil). Nickel sputtering target (2 inches, 99.99%) was purchased from Goodfellow Corporation (Coraopolis, PA, USA). All solvents and reagents were of analytical grade and were used as received.

2.2. Synthesis of SiO$_2$ nanospheres

The silica nanospheres (nSiO$_2$) were prepared as reported elsewhere [36]. In a typical experiment, 178.4 g of IGEPAL CO-520 was dispersed in 2.8 L of cyclohexane and 38 mL of NH$_4$OH (29% aqueous solution) were added to prepare a reverse microemulsion. After adding 30.8 mL of TEOS, the microemulsion was gently stirred for 24 h at room temperature. The nSiO$_2$ was precipitated with methanol and collected by centrifugation at 7000 rpm. After being washed with ethanol, the material was dried at 50 °C for 12 h. The silica nanospheres were calcined in air atmosphere for 2 h at 500 °C in order to remove all organic residues.

2.3. Ni catalyst prepared by magnetron sputtering deposition

The deposition of Ni NPs on the surface of nSiO$_2$ nanospheres was performed by a magnetron sputtering deposition method (Intercovamex-H2). A mechanical resonant agitator was specially designed and placed inside of the vacuum chamber in order to agitate the SiO$_2$ powders during the Ni deposition for a better covering of their surface, as described elsewhere [29–32]. For sputtering deposition, 150 mg of nSiO$_2$ powder was placed into a glass support connected to the mechanical resonant agitator. In each experiment, the sputtering chamber was evacuated to a base pressure of 2.0×10^{-7} mbar for 24 h. The vacuum pressure was adjusted for a sputtering working pressure (argon plasma) of 2.0×10^{-2} mbar by adding ultra pure Argon (99.999%). The working distance between the metal target and the mechanical resonant agitator was 5.0 cm. A vibration frequency of 30 Hz was maintained for revolving the support particles by a sinusoidal wave generation supply during sputtering of a 2-inch nickel target (99.99%). The Ni/nSiO$_2$ catalyst was prepared at 100 W power for 30 min sputtering deposition

time, which corresponds to a metal loading of 2.4 wt%, quantified using flame atomic absorption spectrometry (FAAS).

2.4. Ni catalyst prepared by incipient wetness impregnation

The Ni-IMP/nSiO$_2$ catalyst was prepared by impregnating 300 mg of nSiO$_2$ with 0.6 mL of 0.2 mol L^{-1} aqueous Ni(NO$_3$)$_2$ to prepare 2.4 wt% Ni catalyst. The Ni catalyst was calcined in air (5 h, 550 °C) and reduced under H$_2$ (50 mL min^{-1}) at 500 °C for 3 h before use.

2.5. Catalyst characterization

Catalyst morphology was investigated by the acquisition of bright-field high-resolution images (BF-HRTEM) in an aberration corrected transmission electron microscope FEI Titan Themis operating at 300 kV. The samples were prepared by directly applying the catalyst powder onto standard TEM grids. Small angle X ray scattering (SAXS) experiments were performed at the SAXS1 beam line of Brazilian Synchrotron Light Laboratory (LNLS), with λ = 1.488 Å and 0.05 < q < 3.33 nm^{-1}, where $q = 4\pi.\sin(2\theta)/\lambda$; q is the scattering vector, θ is the scattering angle and λ is the X ray wavelength. The powder samples were cast on Kapton tape by filling homogeneously a stainless-steel washer used as a mold with Kapton tape on both sides. The subtraction of scattering from Kapton windows and air was performed using FIT2D software. Two samples were analysed, one containing pure nSiO$_2$ to investigate their size, shape and structure organization and other containing Ni/nSiO$_2$. The fitting procedures were performed using SASFIT software. The X-ray diffraction (XRD) pattern of the sample was recorded with a Rigaku Miniflex diffractometer using Cu Kα radiation at 2θ = 20–90° with a 0.02° step size. X-ray absorption spectroscopy (XAS) data were performed at the Ni K-edge (8333 eV) in the XAFS1 beam line of the Brazilian Synchrotron Light Laboratory (LNLS) in transmission mode, using a channel-cut Si(111) crystal monochromator and three ionization chambers to detect incident and transmitted photon fluxes. Prior to analysis, the sample (60 mg of Ni/nSiO$_2$, 30 min of Ni sputtering) was pressed into pellets. The data were then acquired in-situ during RWGS reaction under gas mixtures of 1 vol.% CO$_2$ and 4 vol.% H$_2$ in Ar balance, from room temperature to 800 °C. The catalytic reaction was monitored with a mass spectrometer. To ensure the good reproducibility during data collection, the XANES spectra of Ni metal foil were simultaneously measured and the energy was calibrated by aligning the respective absorption edges. The normalization of edge-step data was performed after a linear pre-edge subtraction and the regression of a quadratic polynomial beyond the edge, using ATHENA software [37,38]. Standard spectra of NiO and Ni(0) were collected under the same experimental conditions, using sample position for investigation of the presence of NiO in the NPs by Linear Combination Fittings (LCF). The LCF of the Ni K-edge XANES spectra were conducted within a range of −20 to 30 eV with the normalized E$_0$ spectra using Athena – IFEFFIT software package [38]. X-ray photoelectron spectroscopy (XPS) spectra were obtained using conventional equipment with a high-performance hemispheric analyzer (VG Escalab 220 XL spectrometer) with monochromatic Al Kα (h ν = 1486.6 eV) radiation as the excitation source. The operating pressure in the ultra-high vacuum chamber (UHV) during the analysis was 10^{-9} Pa. Energy step of 20 eV was used for the single-element spectra. Peak decomposition was performed using a 70% Gaussian type curve and a 30% Lorentzian type curve, and a Shirley-type baseline. Si2p and C1 s peaks were also monitored to check for charge stability as a function of time. The C1 s peak of adventitious carbon was fixed at 284.8 eV to set the binding energy scale, and the data treatment was performed using CasaXPS software (Casa Software Ltd., UK).
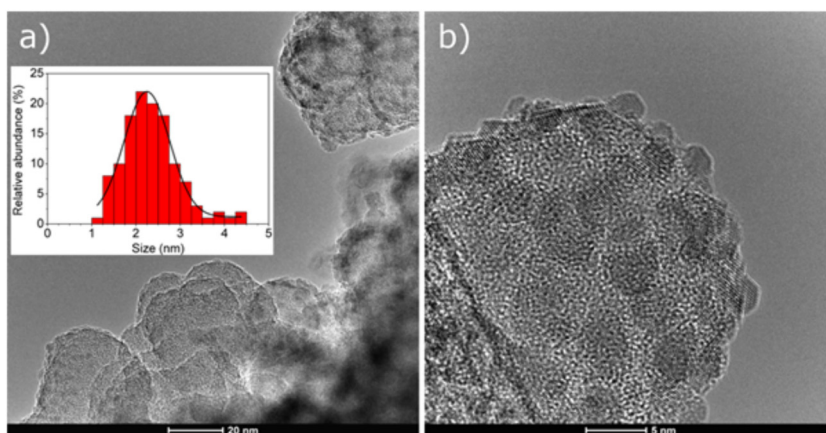
Fig. 1. Bright-field HRTEM images of Ni/nSiO$_2$ prepared by 30 min of sputtering deposition time. The inset shows the size distribution histogram.

2.6. Catalytic reactions

The RWGS reaction was performed on an Integrated Microreactor-MS system equipped with a CATLAB-PCS Module and a QIC-20 MS Module (Hiden Analytical, UK) using 15 mg of Ni/nSiO$_2$ catalyst powder placed in a quartz tube reactor (length: 200 mm, width: 5 mm). Different flow reactant mixture containing 2 vol.% CO$_2$ and 8 vol.% H$_2$ in Ar balance or 2 vol.% CO$_2$ and 2 vol.% H$_2$ in Ar balance was passed through the reactor at a total flow rate of 100 mL min^{-1} and heated at 10 °C/min from room temperature to 800 °C. The gas composition in percentage was obtained from response factor (RF) mass signals using Ar (m/z 40 amu) signal as an internal standard. The RWGS reaction was studied using a Diffuse Reflectance Infrared Fourier Transform (DRIFT) cell from Pike Technologies (Heat chamber for Diffuse IR). The catalyst powder was placed onto a sampling cup. The gas was admitted into the chamber through gas flow meters at the composition of 1:4 CO$_2$:H$_2$ balanced to 50 mL min^{-1} with Ar. Fourier transform infrared (FTIR) spectra were collected at isotherms of 200, 430 and 660 °C. The FTIR spectra were recorded using a Shimadzu IR-Affinity equipped with a KBr beamsplitter and the spectra were collected with a spectral resolution of 4 cm^{-1} and 1000 scans.

3. Results and discussion

3.1. Catalyst preparation and characterization

The catalyst support chosen was comprised of silica nanospheres (nSiO$_2$) with a mean diameter of 18.4 nm and only 3.6% of size dispersion, as determined by SAXS measurements (Fig. S1, see supplementary material for details), obtained by a reverse microemulsion method [36]. The small support particles' size provides an enhanced surface area for metal deposition by the magnetron sputtering technique and the high degree of homogeneity of the material will certainly contribute for the reproducibility of the catalyst preparation method. During the sputtering deposition process, Ni atoms or clusters were ejected from the sputter target (Ni 99.99%) and deposited onto the surface of the nSiO$_2$ nanospheres. The sputtering chamber is equipped with a mechanical resonant agitator system, which permits the vibration of the nSiO$_2$ nanospheres for an homogenous deposition of metal on the support [29]. The Ni/nSiO$_2$ catalyst obtained after 30 min of sputtering deposition contains 2.4 wt% Ni (determined by FAAS). The preparation was repeated and similar nickel loadings were obtained from different batches. High-resolution transmission electron microscopy (HRTEM) analysis revealed the shape and size of Ni/nSiO$_2$ catalyst. Fig. 1 shows that the nSiO$_2$ support
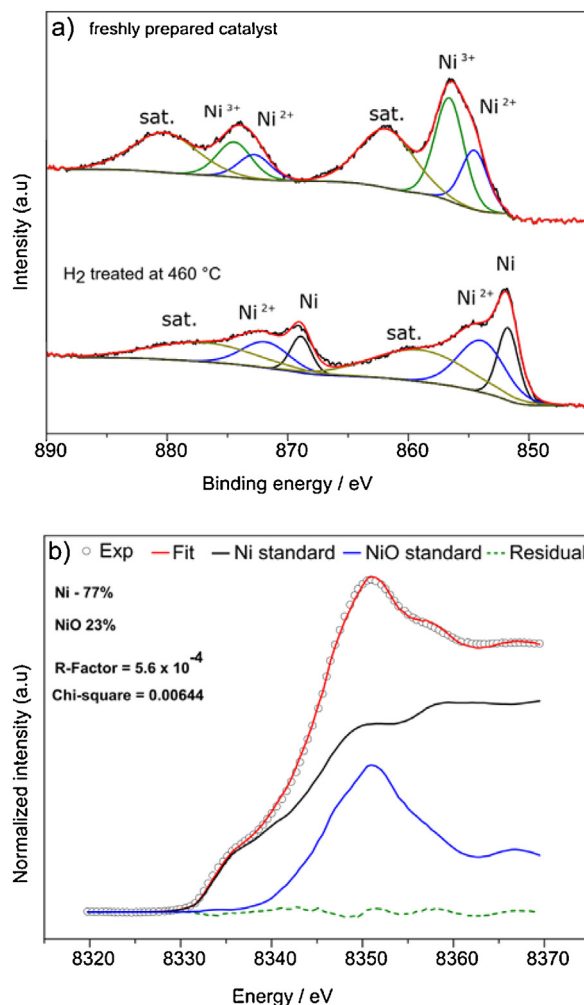
Fig. 2. a) Ni 2p XPS region for freshly prepared Ni/nSiO$_2$ catalyst and for Ni/nSiO$_2$ catalyst treated with H$_2$ at 460 °C and b) Ni K-edge for freshly prepared Ni/nSiO$_2$ catalyst.

consisted of spherical particles, as determined by SAXS, and was decorated with nickel nanoparticles with an average size of 2.3 nm.

The XPS spectrum of the Ni 2p region shown in Fig. 2a was used to investigate the chemical state of Ni present in the freshly prepared Ni/nSiO$_2$ catalyst surface. The XPS spectra of the O1s, Si2p and C 1 s regions were presented in the Supplementary Material (Fig. S2). Generally, the binding energies and their chemical shifts

in XPS spectra are sufficient to determine the oxidation states of surface nickel species. Indeed, as reported in the literature, the XPS peaks in Ni 2p region at about 856.0 eV and 862.0 eV are assigned to Ni^{2+} and Ni^{2+} satellite components, respectively [39,40]. However, very often these assignments can be compromised by the multiplet contributions in oxides as well as by satellite structures observed at higher binding energy. The Ni 2p curve fitted data indicate the presence of Ni^{2+} and Ni^{3+} (main peaks at 854.5 eV and 856.6 eV, respectively) and a satellite peak (at 861.8 eV) in Fig. 2a. The presence of nickel oxide on the surface of as-prepared sample is probably due to the oxidation of nickel during storage in air. This oxidation may be complete (bulk oxidation), partial (core-shell structures) or on the most external supported metal nanoparticles only (passivation due to the oxygen adsorption). Metallic nickel was not detected on the surface of the freshly prepared Ni/nSiO$_2$ sample by XPS, but it was confirmed after analysis of the sample bulk composition by XAS and XRD. These differences could be explained by the way deposition of nickel occurs during the sputtering process, leading to regions with superposition of the very small Ni particles on the support. Ni particles localized near to the surface may contribute the metallic character seen by XAS and those at the top undergo oxidation. Additional XPS analysis on Ni/nSiO$_2$ sample treated with H$_2$ at 460 °C (Fig. 2a) revealed main peaks at 851.7 and 853.9 eV, which were assigned to Ni^0 and Ni^{2+}, respectively, confirming the coexistence of oxidized and reduced nickel species on the catalyst surface [35,36].

The local atomic structure properties of the freshly prepared Ni/nSiO$_2$ NPs were probed by X-ray absorption near-edge structure (XANES). Fig. 2b displays the normalized Ni K-edge XANES spectrum of the freshly-prepared sample and reference materials (Ni and NiO) measured at room temperature. The pre-edge peak at about 8335 eV is very similar to that of standard Ni metal spectrum. This pre-edge feature suggests that the sample shortly after sputtering deposition has a Ni metallic character. Indeed, the Linear Combination Fitting (LCF) simulation of the XANES spectrum revealed a phase percentage of 77 and 23% of Ni and NiO, respectively, that is in good agreement with the energy position of the pre-edge feature [41]. The presence of 23% of NiO in the freshly-prepared sample is due to the oxidation of Ni to NiO after air exposure of the samples. The LCF fit quality was available by the R and χ^2 factors, which are in good agreement with the expected values [42]. From the XRD pattern (Fig. S3 in the Supplementary Material), the diffraction peaks located at 2θ 44.5, 51.9 and 76.4° could be assigned to the (1 1 1), (2 0 0) and (2 2 0) planes of Ni(0) with a cubic structure and space group of Fm–3 m (PDF file 87-712). Due to the low metal loading and small particle size (~2.3 nm), the diffraction peaks are very broad, suggesting a highly dispersed Ni(0) metal phase on the surface of nSiO$_2$ support. No other crystalline phase was observed by XRD analysis.

3.2. Catalytic studies

The Ni/nSiO$_2$ catalyst was employed in the RWGS reaction using 1:1 and 1:4 (CO$_2$:H$_2$) gas composition and the results are displayed in Fig. 3. The RWGS reaction $(CO_2 + H_2 \rightleftharpoons CO + H_2O)$ starts to produce CO at ~200 °C and was predominant in the whole temperature range studied. The methanation reaction $(CO_2 + 4H_2 \rightleftharpoons CH_4 + 2H_2O)$ occurred concomitantly at temperatures between 300 and 600 °C. The reaction performed in excess of H$_2$ reached up to 74% of CO$_2$ conversion into CO (at 800 °C) and a maximum of CH$_4$ (up to 10%) at 430 °C. The production of CH$_4$ is very low (1.3%) for the reaction performed with CO$_2$:H$_2$ of 1:1, while the CO$_2$ conversion reached 50% at 800 °C. Above 600 °C, CO was the only product observed and the conversion of CO$_2$ was close to the thermodynamic equilibrium values for 1:1 and 1:4 (CO$_2$:H$_2$) gas composition (Fig. S4, see Supplementary Mate-
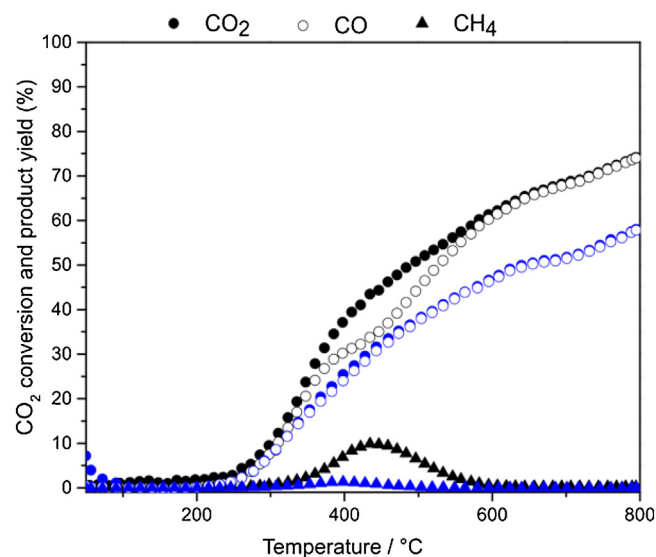

Fig. 3. CO$_2$ conversion and CO and CH$_4$ formation on Ni/nSiO$_2$ catalyst as a function of temperature using different CO$_2$:H$_2$ ratio: 1:4 (black) and 1:1 (blue). (For interpretation of the references to colour in this figure legend, the reader is referred to the web version of this article.)
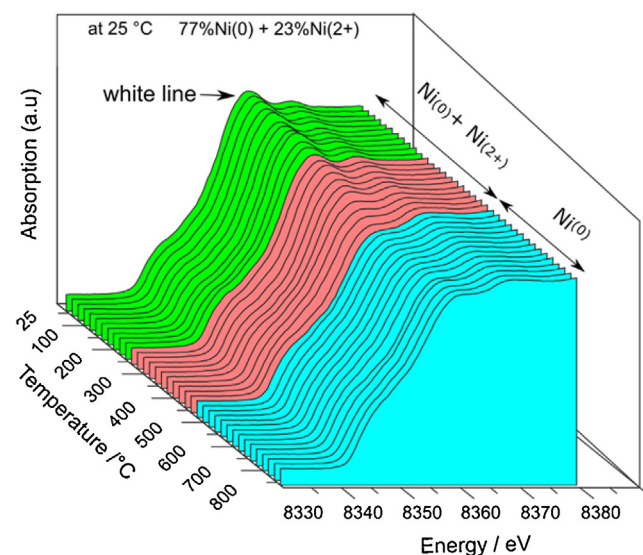

Fig. 4. Evolution of Ni-K edge for *in-situ* XANES spectra of Ni/nSiO$_2$ catalyst during RWGS reaction.

rial). Luhui et al. [19] reported that the yield of CH$_4$ progressively increased with increasing nickel content and suggested that highly dispersed nickel particles (along with oxygen vacancies) are the key active components for RWGS and bulk nickel particles are the main active sites for methanation of CO$_2$. The Ni/nSiO$_2$ catalyst is more active for the RWGS and less active for the methanation reaction, which is a strong evidence that the magnetron sputtering deposition method is able to produce highly dispersed nickel particles. The maximization of metal loading and minimization of aggregates is very important for the design of more active and selective nickel catalysts [43].
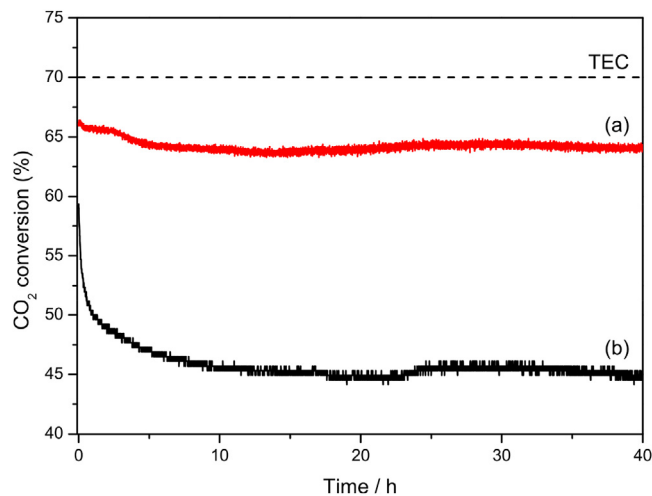
In-situ XANES was used here to determine the active phase of Ni/nSiO$_2$ catalyst at different temperatures while the catalyst was submitted to the RWGS reaction conditions. Fig. 4 shows the in-situ XANES measurement under operando RWGS reaction conditions (CO$_2$:H$_2$ 1:4) as a function of temperature. The XANES spectra for the sample heated up to 250 °C under RWGS reaction conditions
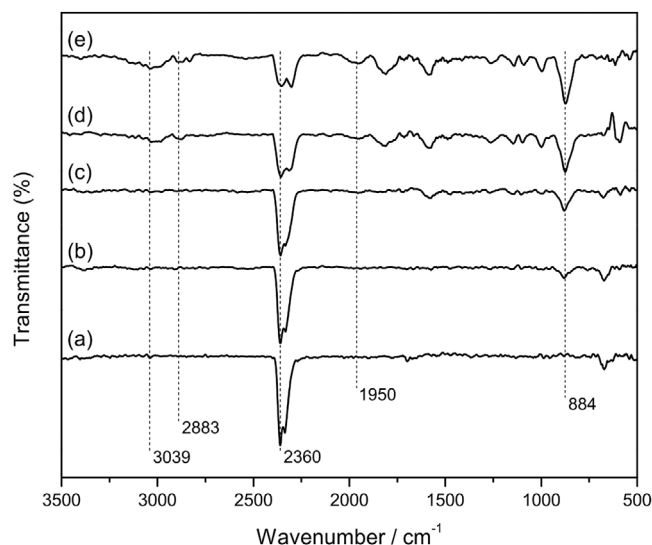
Fig. 5. In situ DRIFT spectra performed at (a) 35 °C, (b) 100 °C, (c) 200 °C, (d) 430 °C and (e) 660 °C with gas mixture of 1:4 (CO_2:H_2) balanced with Ar to a total flow of 50 mL min^{-1}.

Fig. 6. Time on stream stability of (a) Ni/nSiO$_2$ (after a heating cycles until 800 °C) and (b) Ni-IMP/nSiO$_2$ catalysts in the RWGS reaction at 660 °C with a gas mixture of 1:4 (CO_2:H_2). TEC = thermodynamic equilibrium conversion at 660 °C and 1:4 (CO_2:H_2).

suggest that at this stage the catalyst does not suffer strong structural changes, indicating that the mixture of Ni(0)/NiO phases is maintained. The catalytic results shown in Fig. 3 also suggest that CO_2 conversion is minimal bellow 250 °C. After a further increase of the temperature, the CO_2 conversion increased substantially at temperatures above 250 °C (see Fig. 3). The in-situ XANES result showed that the reduction of NiO phase started at this temperature, as can be noticed by the decrease of the white line intensity at 8350 eV, suggesting that NiO was converted into Ni under RWGS reaction conditions. The reduction of NiO to Ni(0) is likely due to the excess of H_2 present in the flow of the reactant mixture (CO_2:H_2 1:4). Above 500 °C, the XANES spectra did not show any considerable change, which indicates the complete reduction of nickel in the temperature range from 250 to 500 °C under the RWGS conditions.

In-situ diffusive reflectance infrared Fourier Transform spectroscopy (DRIFTS) analysis was performed to shed some light on the species formed on the catalyst surface under RWGS conditions. The measurements were performed at 200, 430 and 660 °C with the gas mixture of 1:4 (CO_2:H_2) balanced with Ar to a total flow of 50 mL min^{-1} (Fig. 5). Multiple bands appeared in the region from 1800 to 1000 cm^{-1} and were mostly due to the symmetric and asymmetric stretching vibration modes of the O—C—O group of carboxylate, formate and/or carbonate species [44–46]. The intense bands around 2360 cm^{-1} are present in all spectra and were due to gas-phase and possibly some weakly adsorbed CO_2. The bands at 3039 and 2883 cm^{-1} which appeared after 430 °C can be attributed to the stretching and bending vibration of the C—H bond, indicating the presence of formate species on the catalyst surface. The band at 884 cm^{-1} can be attributed to an out-of-plane bending vibration of carbonate species that are formed at temperature as low as 100 °C. The band at 1950 cm^{-1} can be attributed to a stretching vibration mode of carbonyl (expected at 2000–2050 cm^{-1}). The shift in energy indicates low coverage of CO on the metal surface (bidentated coordination mode) [47]. The formate species are not initially detected (at the temperature where the catalyst is inactive) but are well evidenced on the catalyst at T ≥ 430 °C, which may indicate a reduction of hydrogenate carbonates into formate species. The formation of carboxyl and formate species at the catalyst surface upon heating the catalyst in the presence of the reaction gas mixture (CO_2/H_2) suggests that these species are reaction intermediates. The CO formation is always significantly higher than CH$_4$ forma-

tion, suggesting that the hydrogenation of formate intermediates into CH$_4$ is less favorable to occur on the Ni/nSiO$_2$ catalyst.

The stability of the Ni/nSiO$_2$ catalyst after a heating cycles until 800 °C was evaluated at 660 °C with a gas mixture of 1:4 (CO_2:H_2). Methane is not produced at this temperature and the conversion of CO_2 into CO decreased from 66 to 64% after the first 5 h and then was maintained at 64% with 100% selectivity to CO (Fig. 6a). This behavior represents an excellent stability for 40 h on stream. For comparison, a Ni catalyst was prepared by the traditional incipient wetness impregnation method using the same support and metal loading. The Ni-IMP/nSiO$_2$ catalyst showed a lower initial conversion (57%) and a pronounced drop in activity, reaching 45% conversion after 10 h, than the catalyst prepared by the sputtering deposition method. After operation for 20 h at 660 °C, the Ni/nSiO$_2$ catalyst exhibits a higher specific activity of 2.6 mmolCO$_2$ g-Ni^{-1} s^{-1} when compared with the Ni-IMP/nSiO$_2$ catalyst that reached 1.8 mmolCO$_2$ g-Ni^{-1} s^{-1}. The higher stability for long time on stream (3% vs. 30% drop in conversion) and the higher activity are both important features of the Ni catalyst obtained by the sputtering deposition method.

The thermal stability of both catalysts was also investigated by performing two successive heating cycles until 800 °C using the same gas mixture of 1:4 (CO_2:H_2) (Fig. 7). After the first catalytic test (heating up to 800 °C), the catalysts were cooled down below 50 °C and a new heating ramp up to 800 °C was performed. The Ni-IMP/nSiO$_2$ catalyst prepared by the incipient wetness impregnation was less active than the Ni/nSiO$_2$ catalyst prepared by sputtering deposition method in the whole temperature range studied. A significant shift in the temperature where the reaction starts (∼100 °C higher) was observed for both catalysts in the second cycle. However, a more pronounced difference in the catalysts performance was observed at high temperature (between 600 to 800 °C) in the second RWGS reaction cycle. The Ni/nSiO$_2$ catalyst reached the same conversion of the first cycle, but the Ni-IMP/nSiO$_2$ catalyst deactivated at temperatures >500 °C. Those results agree well with the stability shown in Fig. 6. Moreover, the spent Ni/nSiO$_2$ catalyst produces undetectable amount of methane, which suggests that the methanation reaction was blocked due to changes that may have occurred on the catalyst surface during the first heating ramp. Analysis of the spent Ni/nSiO$_2$ catalyst by STEM revealed sintering of the Ni particles submitted to the heating cycle (Fig. S4, see supplementary material). The changes of the metal phase during elevated temperature tests (up to 800 °C) did not affect the reac-
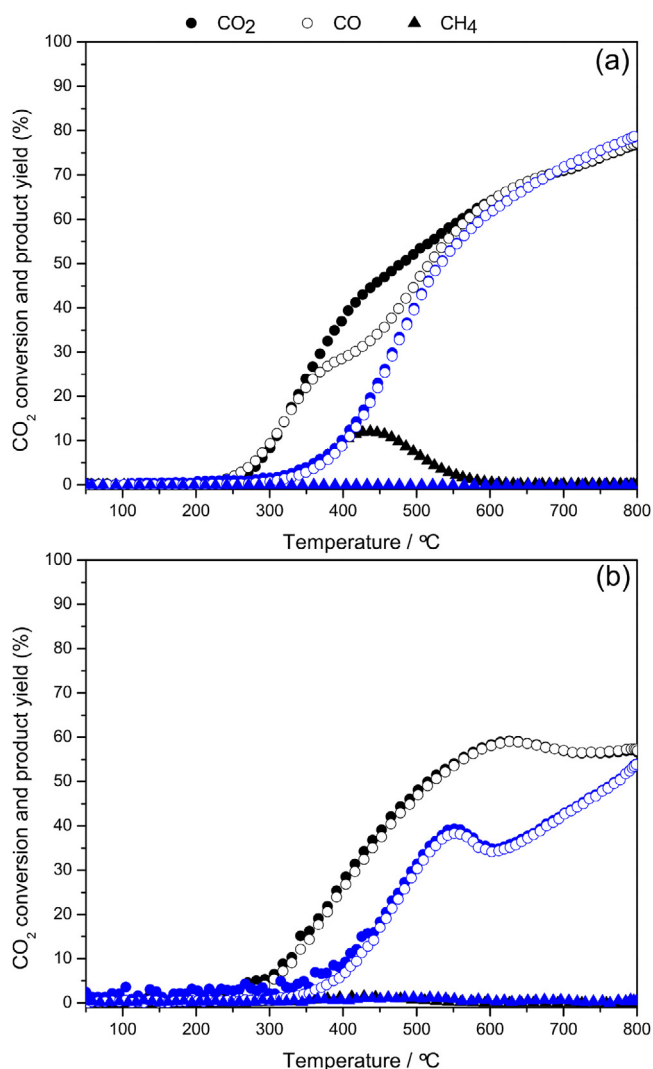
Fig. 7. First (black) and second (blue) RWGS reaction cycle using (a) Ni/nSiO$_2$ and (b) Ni-IMP/nSiO$_2$ catalysts with a gas mixture of 1:4 (CO$_2$:H$_2$). After a first heating cycle until 800 °C the catalysts were cooled down to room temperature under Ar. (For interpretation of the references to colour in this figure legend, the reader is referred to the web version of this article.)

tivity of Ni/nSiO$_2$ catalyst at temperature >600 °C. We do not have a clear explanation for the suppression of the methanation reaction in the temperature range studied, since it is usually associated to an increase of metal dispersion [24,25]. Different effects of CO on nickel catalysts have been previously described, either involving dispersion of the metallic nickel phase in the catalyst with a decrease in the size of Ni particles [48] or sintering of the nickel particles [49,50] over the course of the reaction. This behavior is interesting and should be clarified in detail in future studies using DRIFTS CO chemisorption to characterize catalytic sites that may be undetected with traditional transmission electron microscopy.

4. Conclusions

The magnetron sputtering deposition method allowed the straightforward and fast deposition of nickel on silica powder producing, in 30 min, dispersed nickel particles with an enhanced selectivity for the RWGS reaction. The freshly prepared catalyst contains 77% Ni and 23% NiO phases, due to surface oxidation. In-situ XAS analysis showed that the minor NiO phase was reduced under the RWGS reaction conditions. The CO$_2$ reduction profile

showed that conversion starts at T > 200 °C and reached 74% (1:4 CO$_2$:H$_2$) or 50% (1:1 CO$_2$:H$_2$) at 800 °C. Those values are close to the thermodynamic equilibrium conversion (TEC) for RWGS reaction. Methane was concomitantly formed at lower temperatures at low yields (max. yield 10% (1:4 CO$_2$:H$_2$) or 1.3% (1:1 CO$_2$:H$_2$) at 430 °C), but is suppressed in the second reaction cycle. The catalytic performance, evidenced by the activity at T > 600 °C and stability for a long time on stream, is superior to that of a classical catalyst prepared by incipient wetness impregnation. The maximization of metal loading and minimization of aggregates is very important for the design of more active and selective nickel catalysts for the RWGS reaction. The selective conversion of CO$_2$ into CO is the first step towards the production of liquid fuels via the FT process. An important feature of the sputtering technique is the possibility to tune the metal loading by simply increasing the sputtering time. The sputtering technique is readily applicable also to different supports and has an enormous potential for the preparation of supported metal particle catalysts.

Appendix A. Supplementary data

Supplementary data associated with this article can be found, in the online version, at http://dx.doi.org/10.1016/j.apcatb.2017.02.081.

References

[1] G. Centi, E.A. Quadrelli, S. Perathoner, Catalysis for CO$_2$ conversion: a key technology for rapid introduction of renewable energy in the value chain of chemical industries, Energy Environ. Sci. 6 (2013) 1711–1731.

[2] S. Saeidi, N.A.S. Amin, M.R. Rahimpour, Hydrogenation of CO$_2$ to value-added products—a review and potential future developments, J. CO$_2$ Util. 5 (2014) 66–81.

[3] M. Mikkelsen, M. Jorgensen, F.C. Krebs, The teraton challenge. A review of fixation and transformation of carbon dioxide, Energy Environ. Sci. 3 (2010) 43–81.

[4] Q. Liu, L. Wu, R. Jackstell, M. Beller, Using carbon dioxide as a building block in organic synthesis, Nat. Commun. 6 (2015) 5933.

[5] P. Kaiser, R.B. Unde, C. Kern, A. Jess, Production of liquid hydrocarbons with CO$_2$ as carbon source based on reverse water-gas shift and Fischer-Tropsch synthesis, Chem. Ing. Tech. 85 (2013) 489–499.

[6] A.A. Olajire, Valorization of greenhouse carbon dioxide emissions into value-added products by catalytic processes, J. CO$_2$ Util. 3–4 (2013) 74–92.

[7] G. Centi, S. Perathoner, Opportunities and prospects in the chemical recycling of carbon dioxide to fuels, Catal. Today 148 (2009) 191–205.

[8] W. Wang, S. Wang, X. Ma, J. Gong, Recent advances in catalytic hydrogenation of carbon dioxide, Chem. Soc. Rev. 40 (2011) 3703–3727.

[9] Y.A. Daza, R.A. Kent, M.M. Yung, J.N. Kuhn, Carbon dioxide conversion by reverse water–gas shift chemical looping on perovskite-type oxides, Ind. Eng. Chem. Res. 53 (2014) 5828–5837.

[10] P.C. Zonetti, S. Letichevsky, A.B. Gaspar, E.F. Sousa-Aguiar, L.G. Appel, The Ni$_x$Ce$_{0.75}$Zr$_{0.25-x}$O$_2$ solid solution and the RWGS, Appl. Catal. A Gen. 475 (2014) 48–54.

[11] Y.A. Daza, J.N. Kuhn, CO$_2$ conversion by reverse water gas shift catalysis: comparison of catalysts, mechanisms and their consequences for CO$_2$ conversion to liquid fuels, RSC Adv. 6 (2016) 49675–49691.

[12] K. Kitamura Bando, K. Soga, K. Kunimori, H. Arakawa, Effect of Li additive on CO$_2$ hydrogenation reactivity of zeolite supported Rh catalysts, Appl. Catal. A Gen. 175 (1998) 67–81.

[13] H. Kusama, K.K. Bando, K. Okabe, H. Arakawa, CO$_2$ hydrogenation reactivity and structure of Rh/SiO$_2$ catalysts prepared from acetate, chloride and nitrate precursors, Appl. Catal. A Gen. 205 (2001) 285–294.

[14] Y. Liu, D.Z. Liu, Study of bimetallic Cu-Ni/gamma-Al$_2$O$_3$ catalysts for carbon dioxide hydrogenation, Int. J. Hydrogen Energy 24 (1999) 351–354.

[15] C.-S. Chen, W.-H. Cheng, S.-S. Lin, Study of reverse water gas shift reaction by TPD, TPR and CO$_2$ hydrogenation over potassium-promoted Cu/SiO$_2$ catalyst, Appl. Catal. A Gen. 238 (2003) 55–67.

[16] C.-S. Chen, W.-H. Cheng, S.-S. Lin, Enhanced activity and stability of a Cu/SiO$_2$ catalyst for the reverse water gas shift reaction by an iron promoter, Chem. Commun. (2001) 1770–1771.

[17] C.-S. Chen, W.-H. Cheng, S.-S. Lin, Study of iron-promoted Cu/SiO$_2$ catalyst on high temperature reverse water gas shift reaction, Appl. Catal. A Gen. 257 (2004) 97–106.

[18] C.S. Chen, J.H. Lin, J.H. You, C.R. Chen, Properties of Cu(thd)$_2$ as a precursor to prepare Cu/SiO$_2$ catalyst using the atomic layer epitaxy technique, J. Am. Chem. Soc. 128 (2006) 15950–15951.

[19] L. Wang, S. Zhang, Y. Liu, Reverse water gas shift reaction over Co-precipitated Ni-CeO$_2$ catalysts, J. Rare Earths 26 (2008) 66–70.

[20] F.-m. Sun, C.-f. Yan, Z.-d. Wang, C.-q Guo, S.-l Huang, Ni/Ce–Zr–O catalyst for high CO$_2$ conversion during reverse water gas shift reaction (RWGS), Int. J. Hydrogen Energy 40 (2015) 15985–15993.

[21] B. Lu, K. Kawamoto, Preparation of mesoporous CeO$_2$ and monodispersed NiO particles in CeO$_2$, and enhanced selectivity of NiO/CeO$_2$ for reverse water gas shift reaction, Mater. Res. Bull. 53 (2014) 70–78.

[22] L. Wang, H. Liu, Y. Liu, Y. Chen, S. Yang, Effect of precipitants on Ni-CeO$_2$ catalysts prepared by a co-precipitation method for the reverse water-gas shift reaction, J. Rare Earths 31 (2013) 969–974.

[23] L. Wang, H. Liu, Y. Liu, Y. Chen, S. Yang, Influence of preparation method on performance of Ni-CeO$_2$ catalysts for reverse water-gas shift reaction, J. Rare Earths 31 (2013) 559–564.

[24] J.H. Kwak, L. Kovarik, J. Szanyi, Heterogeneous catalysis on atomically dispersed supported metals: CO$_2$ reduction on multifunctional Pd catalysts, ACS Catal. 3 (2013) 2094–2100.

[25] J.H. Kwak, L. Kovarik, J. Szanyi, CO$_2$ reduction on supported Ru/Al$_2$O$_3$ catalysts: cluster size dependence of product selectivity, ACS Catal. 3 (2013) 2449–2455.

[26] H.C. Wu, Y.C. Chang, J.H. Wu, J.H. Lin, I.K. Lin, C.S. Chen, Methanation of CO$_2$ and reverse water gas shift reactions on Ni/SiO$_2$ catalysts: the influence of particle size on selectivity and reaction pathway, Catal. Sci. Technol. 5 (2015) 4154–4163.

[27] S. Abelló, C. Berrueco, D. Montané, High-loaded nickel–alumina catalyst for direct CO$_2$ hydrogenation into synthetic natural gas (SNG), Fuel 113 (2013) 598–609.

[28] A. Westermann, B. Azambre, M.C. Bacariza, I. Graça, M.F. Ribeiro, J.M. Lopes, C. Henriques, Insight into CO$_2$ methanation mechanism over NiUSY zeolites: an operando IR study, Appl. Catal. B: Environ. 174–175 (2015) 120–125.

[29] R.V. Gonçalves, R. Wojcieszak, H. Wender, C. Sato, B. Dias, L.L.R. Vono, D. Eberhardt, S.R. Teixeira, L.M. Rossi, Easy access to metallic copper nanoparticles with high activity and stability for CO oxidation, ACS Appl. Mater. Interfaces 7 (2015) 7987–7994.

[30] R.V. Gonçalves, R. Wojcieszak, P.M. Uberman, D. Eberhardt, E. Teixeira-Neto, S.R. Teixeira, L.M. Rossi, Catalytic abatement of CO over highly stable Pt supported on Ta$_2$O$_5$ nanotubes, Catal. Commun. 48 (2014) 50–54.

[31] R. Bussamara, D. Eberhardt, A.F. Feil, P. Migowski, H. Wender, D.P. de Moraes, G. Machado, R.M. Papaleo, S.R. Teixeira, J. Dupont, Sputtering deposition of magnetic Ni nanoparticles directly onto an enzyme surface: a novel method to obtain a magnetic biocatalyst, Chem. Commun. 49 (2013) 1273–1275.

[32] L. Luza, A. Gual, D. Eberhardt, S.R. Teixeira, S.S.X. Chiaro, J. Dupont, Imprinting catalytically active Pd nanoparticles onto ionic-liquid-modified Al$_2$O$_3$ supports, ChemCatChem 5 (2013) 2471–2478.

[33] G.M. Veith, A.R. Lupini, S.J. Pennycook, A. Villa, L. Prati, N.J. Dudney, Magnetron sputtering of gold nanoparticles onto WO$_3$ and activated carbon, Catal. Today 122 (2007) 248–253.

[34] G.M. Veith, A.R. Lupini, S.J. Pennycook, G.W. Ownby, N.J. Dudney, Nanoparticles of gold on γ-Al$_2$O$_3$ produced by dc magnetron sputtering, J. Catal. 231 (2005) 151–158.

[35] Y. Hatakeyama, K. Onishi, K. Nishikawa, Effects of sputtering conditions on formation of gold nanoparticles in sputter deposition technique, RSC Adv. 1 (2011) 1815–1821.

[36] M.J. Jacinto, P.K. Kiyohara, S.H. Masunaga, R.F. Jardim, L.M. Rossi, Recoverable rhodium nanoparticles: synthesis, characterization and catalytic performance in hydrogenation reactions, Appl. Catal. A Gen. 338 (2008) 52–57.

[37] M. Newville, IFEFFIT: interactive XAFS analysis FEFF fitting, J. Synchrotron Rad. 8 (2001) 322–324.

[38] B. Ravel, M. Newville, ARTEMIS, ATHENA, HEPHAESTUS: data analysis for X-ray absorption spectroscopy using IFEFFIT, J. Synchrotron Rad. 12 (2005) 537–541.

[39] Y.S. Chen, J.F. Kang, B. Chen, B. Gao, L.F. Liu, X.Y. Liu, Y.Y. Wang, L. Wu, H.Y. Yu, J.Y. Wang, Q. Chen, E.G. Wang, Microscopic mechanism for unipolar resistive switching behaviour of nickel oxides, J. Phys. D: Appl. Phys. 45 (2012) 065303.

[40] A.P. Grosvenor, M.C. Biesinger, R.S.C. Smart, N.S. McIntyre, New interpretations of XPS spectra of nickel metal and oxides, Surf. Sci. 600 (2006) 1771–1779.

[41] R.J. Woolley, B.N. Illy, M.P. Ryan, S.J. Skinner, In situ determination of the nickel oxidation state in La$_2$NiO$_{4+δ}$ and La$_4$Ni$_3$O$_{10-δ}$ using X-ray absorption near-edge structure, J. Mater. Chem. 21 (2011) 18592–18596.

[42] F. Meirer, J. Cabana, Y. Liu, A. Mehta, J.C. Andrews, P. Pianetta, Three-dimensional imaging of chemical phase transformations at the nanoscale with full-field transmission X-ray microscopy, J. Synchrotron Rad. 18 (2011) 773–781.

[43] B. Lu, K. Kawamoto, Preparation of monodispersed NiO particles in SBA-15, and its enhanced selectivity for reverse water gas shift reaction, J. Environ. Chem. Eng. 1 (2013) 300–309.

[44] G. Jacobs, L. Williams, U. Graham, D. Sparks, B.H. Davis, Low-temperature water-gas shift: in-situ DRIFTS-reaction study of a Pt/CeO$_2$ catalyst for fuel cell reformer applications, J. Phys. Chem. B 107 (2003) 10398–10404.

[45] T. Tabakova, F. Boccuzzi, M. Manzoli, D. Andreeva, FTIR study of low-temperature water-gas shift reaction on gold/ceria catalyst, Appl. Catal. A Gen. 252 (2003) 385–397.

[46] A. Bourane, O. Dulaurent, D. Bianchi, Heats of adsorption of linear and multibound adsorbed CO species on a Pt/Al$_2$O$_3$ catalyst using in situ infrared spectroscopy under adsorption equilibrium, J. Catal. 196 (2000) 115–125.

[47] B. Qiao, A. Wang, X. Yang, L.F. Allard, Z. Jiang, Y. Cui, J. Liu, J. Li, T. Zhang, Single-atom catalysis of CO oxidation using Pt$_1$/FeO$_x$, Nat. Chem. 3 (2011) 634–641.

[48] V.M. Gonzalez-Delacruz, R. Pereñiguez, F. Ternero, J.P. Holgado, A. Caballero, Modifying the size of nickel metallic particles by H$_2$/CO treatment in Ni/ZrO$_2$ methane dry reforming catalysts, ACS Catal. 1 (2011) 82–88.

[49] W.M. Shen, J.A. Dumesic, C.G. Hill, Criteria for stable Ni particle size under methanation reaction conditions: nickel transport and particle size growth via nickel carbonyl, J. Catal. 68 (1981) 152–165.

[50] M. Agnelli, M. Kolb, C. Mirodatos, CO hydrogenation on a nickel catalyst, J. Catal. 148 (1994) 9–21.